Journal of Zhejiang University-SCIENCE A (Applied Physics & Engineering)
ISSN 1673-565X (Print); ISSN 1862-1775 (Online)
www.zju.edu.cn/jzus; www.springerlink.com
E-mail: jzus@zju.edu.cn

Coal type identification based on the emission spectra of a furnace flame*

Feng YIN[1,2], Zhi-hao LUO[1,2], Yuan LI[1], Ming-xi ZHOU[1], Hao ZHOU[†‡1]

([1]*State Key Laboratory of Clean Energy Utilization, Zhejiang University, Hangzhou 310027, China*)

([2]*Electric Power Research Institute of State Grid Zhejiang Electric Power Company, Hangzhou 310014, China*)

[†]E-mail: zhouhao@zju.edu.cn

Received Nov. 11, 2015; Revision accepted May 27, 2016; Crosschecked Jan. 5, 2017

Abstract: This paper presents a novel method of identifying coal type based on mechanistic methods. The ratio of the resonance line spectrum of a luminous flame and the continuous spectrum at the same wavelength eliminates the influence of temperature on spectral intensity. The atomic line spectra of Na and K are typical and significant over continuous flame spectra. The concentrations of elemental Na and K in the flame are exclusively relative to coal type and composition. Using an experimental furnace and charge-coupled device (CCD) optical spectrometer apparatus, the continuous spectra and atomic line spectra of Na and K elements were sampled from coal flames in real time. An empirical fitting method was used to simplify the formulas of absorption strength and flame temperature calculation, and rational solutions were obtained by using an iterative algorithm. Due to the change in reaction rate and absorption by soot particles, the relative contents of Na and K in a flame vary with the temperature and absorption strength. Arrhenius's equation for temperature compensation was adopted. Compensation for soot density in the furnace was also satisfied by an exponential expression. At any one sampling position, the compensation parameters were identical for all coal types. After compensation for temperature and density of soot particles, the relative strength of the Na and K signals and the ratio between them uniquely matched the coal type burnt in various conditions. The results were replicated and verified in various conditions, and the response time of the system was of the order of seconds.

Key words: Coal type identification; Flame emission spectra; Alkali atomic spectra; Soot density compensation
http://dx.doi.org/10.1631/jzus.A1500306 **CLC number:** TK224.11

1 Introduction

The increasing demand for optimizing coal combustion together with closed-loop control in the combustion of coal-fired power plants has highlighted the need for coal properties to be identified. Tightened economic and environmental constraints have forced power plants to burn an increasingly diverse range of coal types. When a different type of coal is to be fired, its properties therefore need to be determined as quickly as possible. This requires an efficient and rapid method of coal identification in real time. However, at present, most traditional methods of coal analysis used in power plants such as laboratory chemical analysis are still off-line.

Some online methods (e.g., coal analyzers using radiometric, microwave or infra-red (IR) techniques, and passive tagging techniques) are very expensive and require complex installation, as their operation involves either taking samples from the fuel feeding system or detecting tracer particles that have been added to the fuel (Xu *et al.*, 2004).

For online testing, Xu *et al.* (2012) used independent component analysis (ICA) and support vector machine (SVM) techniques to identify the fuel

‡ Corresponding author

* Project supported by the National Basic Research Program (973 Program) of China (No. 2015CB251501) and the National Natural Science Foundation of China (No. 51476137)

ORCID: Hao ZHOU, http://orcid.org/0000-0001-9779-7703

types. Three flame detectors were used to capture the flame oscillation signals from the IR, visible, and ultraviolet spectral bands. The flame features were extracted both in the time and frequency domains from each flame oscillation signal (Tan *et al.*, 2009). However, the flame oscillating features are markedly affected by many factors including firing rate, air/fuel ratio, and coal fineness. Thus, the measured signal consistency is relatively poor, which makes identification very difficult. However, neural networks and SVM techniques are very computation-intensive, affecting their real-time performance.

By comparison, the spectrum of a flame is more stable and consistent, and fundamental research on flame radiation intensity is relatively well developed, together with miniaturized spectrum examination equipment and technology. Low cost, high accuracy, and easily operated spectrometers with charge-coupled device (CCD) detectors are now available (Zhou *et al*., 2015). Typically, current research on flame emission spectrometry has focused on the measurement of flame temperature. From Planck's law linking temperature with radiation intensity, the radiation at two wavelengths may be compared to measure flame temperature (the two-color method). Huang *et al.* (2000) developed an optical instrumentation system for the continuous online measurement of temperatures in a furnace based on the two-color method, and reported experimental results using a 500 kW model furnace. Fu *et al.* (2006) extended two-color pyrometry to three-color pyrometry which does not require calibration, thus avoiding the need to perform prior calibrations required for the geometry of the system. In their study, analysis of measurement uncertainties was also reported (Fu *et al.*, 2010).

In a study of the relationship between the combustion conditions and flame emission spectra, the performance of coal flames was monitored using flame emission spectroscopy (Parameswaran and Hughes, 2007), which indicates how the coal spectral profiles vary with the changes of firing rate and air/fuel ratio. This showed that the shape of the spectral profile has a regular and identifiable relationship with the combustion conditions. Another study using a CCD fiber-optic spectrometer showed that certain characteristic peaks in the flame spectrum are the atomic emission spectra of K and Na, and the flame temperature was measured at the point when these characteristic peaks appeared (Cheng *et al.*, 2004). In a coal flame, most Na and K exists as metallic vapor at high temperature (Takuwa and Naruseb, 2007a). The results of a quantum chemistry study showed that both Na and K are refreshed easily and rapidly from Na_2O/K_2O and NaO/KO by char at high temperature (Wen *et al.*, 2009). The atomic emission spectra of Na and K are distinct in a continuous flame spectrum, and can be used as the identifying tags of a coal flame.

In general, the concentrations and proportions of the various elements in different coal types, including Na and K, are not identical, but are related to the different geological environments during coal formation and the types of coal-forming vegetation. Excepting those present as aluminosilicates, which have a very high melting point and do not readily decompose or evaporate, alkaline metal materials in coal are generally soluble and volatile (Li *et al.*, 2005). In their investigation of the release characteristics of K and Na species during combustion of coal of various rank, Kim *et al.* (2012) suggested that most types of K and Na contained in the fuel were ionized and released, and these existed as KCl or NaCl in the fuel.

Schürmann and Monkhouse (2007), Takuwa and Naruseb (2007a; 2007b), and van Eyk *et al.* (2011) studied the detailed kinetics and behavior of alkaline metal compounds during coal combustion, and showed that, in addition to chlorides, alkali metal vapor released in the furnace process also produces sulfates and hydroxides, and the concentrations of both Na and K are related to the coal ingredients and temperature.

2 Theoretical basis

The energy distribution (i.e., the spectrum) of the spontaneous emission from flames is classified into two types according to their different shapes: continuous and discontinuous spectra. A continuous spectrum is the general form of radiation emitted by the sooty region of rich hydrocarbon flames. Discontinuous spectra, in which the energy is mainly confined around certain narrow wavelengths, are attributed to isolated atoms or molecules (Zizak, 2000). In other words, a line (discontinuous) spectrum represents isolated atoms while a more diffuse (band) spectra represents molecules.

2.1 Fundamentals of atomic emission spectra quantification

A quantitative analysis of spectra is based on the existence of a definite relationship between the concentration of atoms, to be determined, and the intensity of a specific radiation. According to Bohr's theory (Zizak, 2000), energy is emitted when a transition occurs from one energy level, j, to another energy level, i, of an atom, $E_j \rightarrow E_i$. As the energy emitted in any transition is the light quantum hv, for a homogeneous light source of width l and, for the optically thin case, where all radiation escapes, the total emitted line intensity I_l in a spectral line of frequency v per unit solid angle is

$$I_l = \frac{1}{4\pi} hvA_{ji}N_j l = \frac{hc}{4\pi\lambda} A_{ji}N_j l, \tag{1}$$

where h is the Planck constant, c is the speed of light, λ is the wavelength at the line center, A_{ji} is the atomic transition probability, and N_j is the number per unit volume (number density) of excited atoms in the upper (initial) level j (Drake, 1996).

The atomic emission spectral intensity is therefore proportional to the number of excited high-temperature atoms in the flame. For thermodynamic equilibrium, a population of the atomic energy levels according to the (simplified) Boltzmann formula is

$$N_j = N_0 \frac{g_j}{g_0} \exp\left(-\frac{E_j}{KT}\right), \tag{2}$$

where N_0 is the number of ground state atoms per unit volume, g_j and g_0 are the statistical weights of level j and ground state, respectively, which are obtained from the appropriate angular momentum quantum numbers, E_j is the energy of the level j, K is the Boltzmann constant, and T is the temperature.

Planck's law states that the resonance line of an atomic spectrum is $E_j = hv = hc/\lambda$. Therefore, Eqs. (1) and (2) reduce to

$$I_l = \frac{hcg_j A_{ji} l}{4\pi\lambda g_0} N_0 \exp\left(-\frac{hc}{\lambda KT}\right). \tag{3}$$

2.2 Fundamentals of flame emissivity and temperature measurements

The black-body radiation of a flame is given by Plank's law as

$$I_\lambda = \frac{2hc^2}{\lambda^5\{\exp[hc/(\lambda KT)]-1\}}, \tag{4}$$

where I_λ is the intensity at a given wavelength (λ) and temperature (T). When the temperature is in the range of 800–2500 K and the wavelength is in the range of 200–800 nm, $\exp[hc/(\lambda KT)] \gg 1$. Thus, $1/\{\exp[hc/(\lambda KT)]-1\} \approx \exp[-hc/(\lambda KT)]$ (Romero *et al.*, 2005).

Since the furnace environment is not a perfect black body, an additional term for emissivity, ε_λ, at the given wavelength is added to Eq. (4):

$$I_\lambda = \varepsilon_\lambda \frac{2hc^2}{\lambda^5} \exp\left(-\frac{hc}{\lambda KT}\right). \tag{5}$$

For soot particles in the flame, ε_λ is estimated by the widely used empirical correlation (Beatrice *et al.*, 1995):

$$\varepsilon_\lambda = 1 - \exp(-kl/\lambda^\alpha), \tag{6}$$

where k is the integrated absorption coefficient, which is proportional to the soot density, and α is an empirical factor, which has a fixed value of 1.39 for stable flames (Stasio and Massoli, 1994; Zhao and Ladommatos, 1998). From the intensity ratio for two pairs of wavelengths, the kl and T of a flame spectrum can be determined, which is the principle of the two-color pyrometric technique (Huang *et al.*, 2000; Lu and Cheng, 2003).

2.3 Principles of actual flame measurements and coal type identification

In practice, the measured spectra intensities J_l and J_λ are affected by various factors, including the optical sensitivity, observation distance, lens properties, and signal conversion, and are proportional to the real intensities of flame (Huang *et al.*, 2000). Because of these factors, the optical sensitivity S_λ varies with the wavelength, and the others are homologous for every point of a spectrum, which are

expressed as V. The equations are as follows:

$$J_l = S_\lambda V \frac{hcg_j A_{ji} l}{4\pi\lambda g_0} N_0 \exp\left(-\frac{hc}{\lambda KT}\right), \tag{7}$$

$$J_\lambda = S_\lambda V \varepsilon_\lambda \frac{2hc^2}{\lambda^5} \exp\left(-\frac{hc}{\lambda KT}\right). \tag{8}$$

S_λ and V vary in different conditions; however, for the same optical system, the ratio of the values of S_λ is invariant at different wavelengths. This can be calibrated using a standard calibration light source.

For some elements in the flame, the number of ground-state atoms is roughly equivalent to the total number of atoms. If the constituents of the coal are normally distributed, the number of the atoms of any particular element is also proportional to the soot density, given by the integrated absorption coefficient k in Eq. (6). Therefore, letting $N_0=Ck$, where C is the proportion of a specific element in the flame, and relating it to the concentration of that element in the coal, the value of C is characteristic of the coal type and may be used to identify it.

At the wavelengths of the spectral resonance lines of Na and K, dividing Eq. (7) by Eq. (8) would eliminate the influence of temperature, taking Na as an example:

$$\frac{J_{l\text{-Na}}}{J_{\lambda\text{-Na}}} = \frac{\lambda_{\text{Na}}^4 g_{j\text{-Na}} A_{ji\text{-Na}} klC_{\text{Na}}}{8\pi cg_{0\text{-Na}}[1-\exp(-kl/\lambda_{\text{Na}}^\alpha)]}. \tag{9}$$

Letting the constant $\mu_{\text{Na}} = \dfrac{\lambda_{\text{Na}}^4 g_{j\text{-Na}} A_{ji\text{-Na}}}{8\pi cg_{0\text{-Na}}}$ and making C_{Na} the subject of Eq. (9) give

$$C_{\text{Na}} = \frac{1-\exp(-kl/\lambda_{\text{Na}}^\alpha)}{\mu_{\text{Na}} kl} \cdot \frac{J_{\lambda\text{-Na}}}{J_{l\text{-Na}}}. \tag{10}$$

3 Experimental arrangement

The experimental set-up is shown in Fig. 1. A sedimentation furnace test system was used to obtain the ignition temperature, and the combustion and slagging conditions of pulverized coal. The rapid particle-heating rate was relatively similar to that in an actual coal boiler, and very good results were obtained. The ignition and burn-out section are the main part of a sedimentation furnace. Auxiliary equipment included an air compressor, induced draft (ID) fan, ignition oil system, flow control device, coal-powder feeding mechanism, etc. An Ocean Optics Maya2000 Pro spectrometer (HALMA, UK) was used to process the incoming light signals through a fiber-optic probe, shutter, and attenuator system. The spectrometer uses the Hamamatsu S10420 detector. The grating of HC-1 makes the effective range up to 200–1100 nm and it is fitted with a 25 μm slit. A shutter and attenuator filter system to switch and reduce the light intensity was placed in line with the fiber-optic cable to the grating. This allows regulation with the light intensity for better results in the sampling range without saturation. The spectrometer can be connected to various modules and external interfaces, including personal computers, programmable logic controllers, and other embedded controllers, through USB 2.0 communications. Its USB 2.0 interface enables full spectral scans into memory in every 7 ms. The radiometric calibration light source is a calibrated DH-2000 (220–1050 nm).

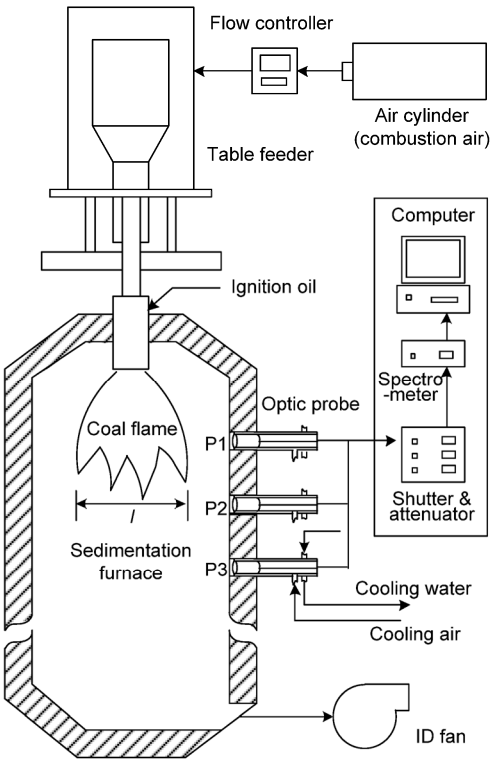

Fig. 1 Experimental arrangement for coal flame emission spectrum detection

Fig. 1 shows the optic probe and CCD spectrometer arrangement. The probe contains a collimating lens for long distances (200–2000 nm), and a fiber-optic cable protected from the high-temperature environment inside the furnace by a water-cooled casing. The collimating lens was mounted at one end of the probe. A small amount of purging air was passed along the inner cylinder of the probe to prevent residue build-up on the window.

Three coal types of different ranks were tested: (1) Datong, (2) Kunlun, and (3) Shenhua. Table 1 shows the proximate analysis and ultimate analysis of these coals, and the coal ash composition is given in Table 2.

4 Results and discussion

Two operating conditions (A and B) are summarized in Table 3, which include sampling position (P1, P3), distance between the probe and the furnace center, coal flow, primary air (PA) velocity, secondary air (SA) velocity, and flow rate ratio of PA and SA (PA/SA ratio). The flame intensity signals sampled from the spectrometer are shown in Figs. 2a and 2b, which include about 100 samples of spectral curve in each graph for the three coal types in two conditions. The spectral curves fluctuate over a large range, which reflects the specific character of the coal flames. The deflagration of coal particles in turbulent air causes the instantaneous temperature and soot density of the coal flame to oscillate. According to Planck's law and Kirchhoff's law of thermal radiation, the shape and size of spectral curves embody the main messages of temperature, emissivity, and soot density. The values extracted from the spectral curve were analyzed after validation treatment. As the single curve in Fig. 3 shows, a signal peak is clearly visible at each of the two wavelengths, 589.0 nm and 766.5 nm. These are the atomic emission spectra of Na and K atoms in the flame. The size of each peak measured above the continuous spectrum represents the element concentrations in the flame, and thus relates to the coal type.

4.1 Temperature and emissivity measurements

Limited by the performance of the spectrometer, the section of the spectral curve in the range of 500–800 nm is steadier and more sensitive, which is more suitable for analysis. The wavelength pairs of 630 nm/670 nm and 600 nm/690 nm were selected for the calculations of temperature and soot density. As shown in Fig. 4 , the optical sensitivity varies with the wavelength. Since the curve is relatively flat

Table 1 Proximate and ultimate analysis of tested coals

Coal type	Proximate analysis (unit: %)				Ultimate analysis (unit: %)					$Q_{ar,net}$ (kJ/kg)
	M_{ad}	A_{ad}	V_{ad}	FC_{ad}	C_{ad}	H_{ad}	N_{ad}	S_{ad}	O_{ad}	
Datong	7.22	9.82	28.56	54.40	68.28	4.90	0.91	0.75	8.83	24876
Kunlun	9.26	24.29	25.02	41.43	52.74	3.76	0.97	0.42	8.56	19649
Shenhua	6.74	9.03	31.10	52.99	68.64	4.11	1.47	0.41	9.58	26340

M: moisture; A: ash; V: volatile; FC: fixed carbon; Q_{net}: net calorific value; ad: air-dried basis; ar: as received basis

Table 2 Chemical compositions of tested coal ash (unit: %)

Coal type	SiO_2	Al_2O_3	Fe_2O_3	CaO	MgO	K_2O	Na_2O	SO_3	K	Na
Datong	48.29	18.04	10.14	8.96	3.86	1.00	0.49	8.24	0.830	0.364
Kunlun	48.26	35.15	6.58	3.45	1.71	0.38	0.22	–	0.315	0.163
Shenhua	46.35	17.18	10.41	20.34	1.37	1.66	1.48	–	1.377	1.098

Table 3 Operating conditions

Condition	Sampling position	Probe distance (m)	Coal flow (kg/h)	PA velocity (m/s)	SA velocity (m/s)	PA/SA ratio
A	P1	0.45	30	7.4	12.7	0.34
B	P3	0.35	30	9.5	11.0	0.39

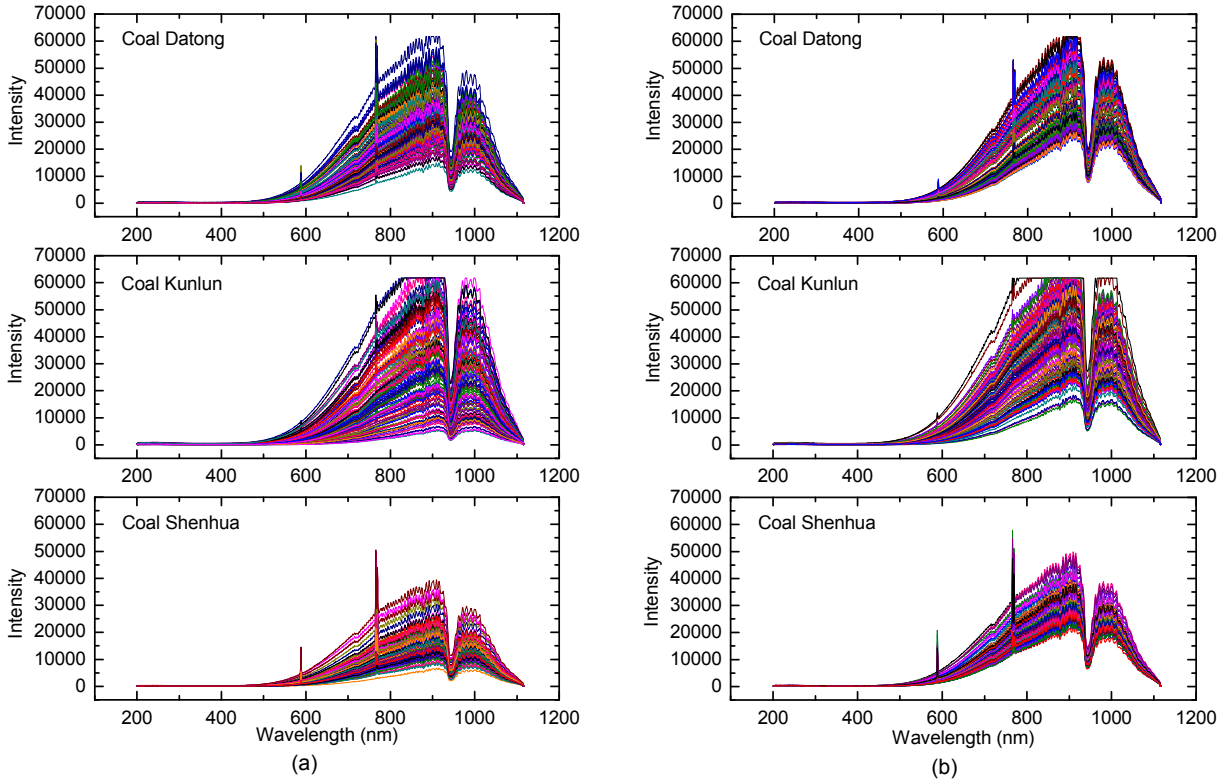

Fig. 2 Flame spectral intensity signals of three coal types sampled from the spectrometer in conditions A (a) and B (b)

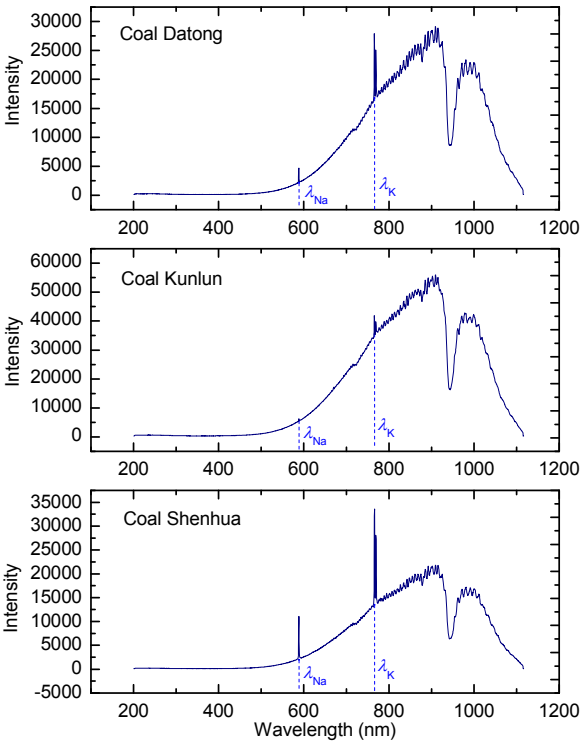

Fig. 3 Typical single flame spectral intensity curve of three coal types

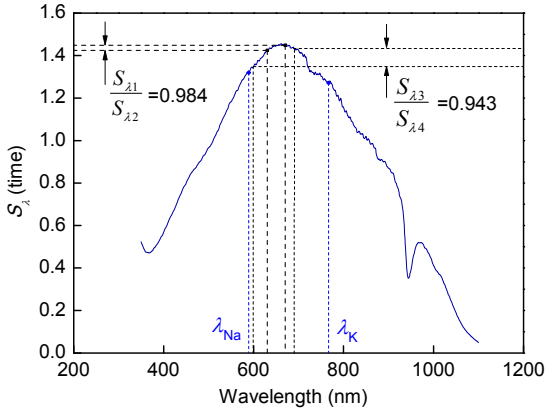

Fig. 4 Optical sensitivity varying with the wavelength

in the range of 600–690 nm, the ratios of sensitivity values in this range are close to 1 and the spectral tendency is closer to the natural status. Rearranging Eq. (8), the temperature for the 630 nm and 670 nm wavelength pair is obtained from

$$T = hc\left(\frac{1}{\lambda_1}-\frac{1}{\lambda_2}\right)\Bigg/\left[K\cdot\ln\left(\frac{S_{\lambda 1}\varepsilon_{\lambda 1}\lambda_2^5 J_{\lambda 2}}{S_{\lambda 2}\varepsilon_{\lambda 2}\lambda_1^5 J_{\lambda 1}}\right)\right], \quad (11)$$

where λ_1=630 nm, λ_2=670 nm, $S_{\lambda1}/S_{\lambda2}$=0.984 as shown in Fig. 4, and $\varepsilon_{\lambda1}/\varepsilon_{\lambda2}=[1-\exp(-kl/\lambda_1^{1.39})]/[1-\exp(-kl/\lambda_2^{1.39})]$ (the unit of the wavelength in this formula is μm).

Letting λ_3=600 nm and λ_4=690 nm, the value of kl can be calculated for a known temperature. To simplify the calculation, instead of the original formula, the fitting formula $\varepsilon_{\lambda3}/\varepsilon_{\lambda4}=[1-\exp(-kl/0.6^{1.39})]/[1-\exp(-kl/0.69^{1.39})]=0.996+\exp(-kl/0.9-1.5)$ was used. The fitted curve was then compared with the original, and the related linear regression coefficient of the formulas is 99.5%. From Eq. (8), kl can be obtained by

$$kl=-0.9\times\left\{\ln\left[\frac{S_{\lambda4}\lambda_3^5 J_{\lambda3}}{S_{\lambda3}\lambda_4^4 J_{\lambda4}}\exp\left(\frac{hc}{KT}\left(\frac{1}{\lambda_3}-\frac{1}{\lambda_4}\right)\right)-0.996\right]+1.5\right\}, \tag{12}$$

where $S_{\lambda3}/S_{\lambda4}$=0.943, as shown in Fig. 4.

Due to the measurement error and signal noise, Eqs. (11) and (12) cannot obtain an exact solution. However, the range of the ratio $\varepsilon_{\lambda1}/\varepsilon_{\lambda2}$ was narrowed down to lie between 1.02 and 1.07 when kl was between 0.2 and 1.4, which is the normal absorption strength range of a luminous flame (Lu and Cheng, 2003). Therefore, an iterative method was used to obtain a locally optimal solution. The ratio $\varepsilon_{\lambda1}/\varepsilon_{\lambda2}$ was selected as the iteration factor. The initial value was 1.02; the number of iterations was 1. One set of measurement results for a coal flame is shown in Fig. 5, which shows a general case of the gray-body radiation of coal flames. It reasonably indicates a relating fluctuant tendency of soot particles temperature and soot concentration (absorption strength).

4.2 Characteristic ratio of K and Na contents

As shown in Fig. 3, the spectral peaks at 589 nm for Na and 766.5 nm for K are both resonance lines. Thus, from Eq. (10) and the National Institute of Standards and Technology (NIST) Atomic Spectra Database (Kramida *et al.*, 2012), we can obtain

$$\mu_{\mathrm{Na}}=\frac{\lambda_{\mathrm{Na}}^4 g_{j\text{-Na}} A_{ji\text{-Na}}}{8\pi c g_{0\text{-Na}}}=1.97\ \mathrm{nm}^3.$$

Likewise,

$$\mu_{\mathrm{K}}=\frac{\lambda_{\mathrm{K}}^4 g_{j\text{-K}} A_{ji\text{-K}}}{8\pi c g_{0\text{-K}}}=3.48\ \mathrm{nm}^3.$$

Then,

$$C_{\mathrm{Na}}=\frac{1-\exp(-kl/0.479)}{1.97kl}\cdot\frac{J_{\lambda\text{-Na}}}{J_{l\text{-Na}}},$$

$$C_{\mathrm{K}}=\frac{1-\exp(-kl/0.691)}{3.48kl}\cdot\frac{J_{\lambda\text{-K}}}{J_{l\text{-K}}}.$$

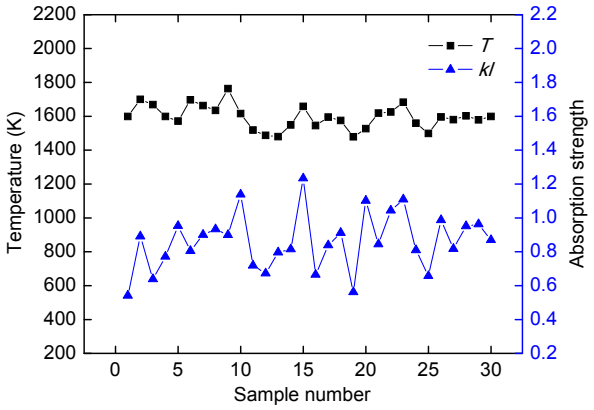

Fig. 5 Measuring results of the temperature and absorption strength of a coal flame

Based on the results in the previous section, the variation trends of C_{Na} and C_{K} versus temperature T and absorption strength kl are shown in Figs. 6 and 7, respectively.

As shown in Figs. 6 and 7, the relative contents of the three coal types vary with temperature T and soot density kl. An Arrhenius-type expression was used to estimate the relationship between reaction rate and temperature (van Eyk *et al.*, 2011). By fitting the experimental data, the empirical temperature compensation factors at temperature T were

$$A_{\mathrm{Na}}=600\exp[-83/(RT)],$$

$$A_{\mathrm{K}}=300\exp[-80/(RT)],$$

where A_{Na} and A_{K} are compensation factors for Na and K at the fixed sampling position, and R is the molar gas constant equal to 0.008 314 51 kJ/(mol·K).

The decreasing relationship depends on the absorption strength, because measurements are attenuated by absorption of light by soot particles. Some photons are absorbed within the flame itself, and

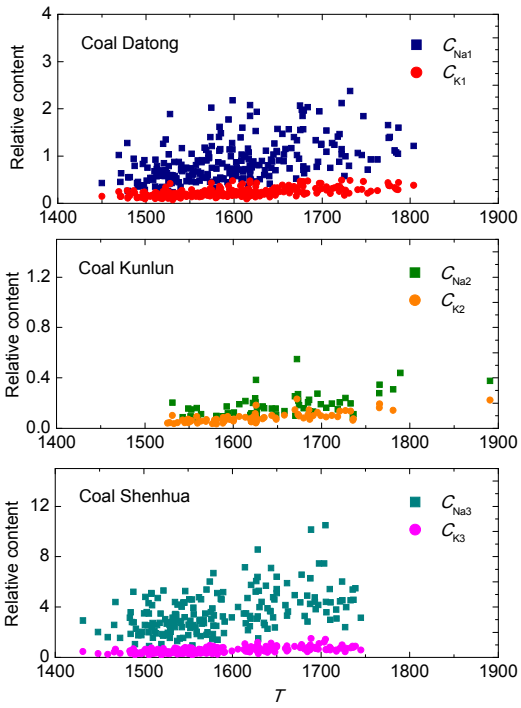

Fig. 6 Relative contents of C_{Na} and C_K versus temperature for three coal types

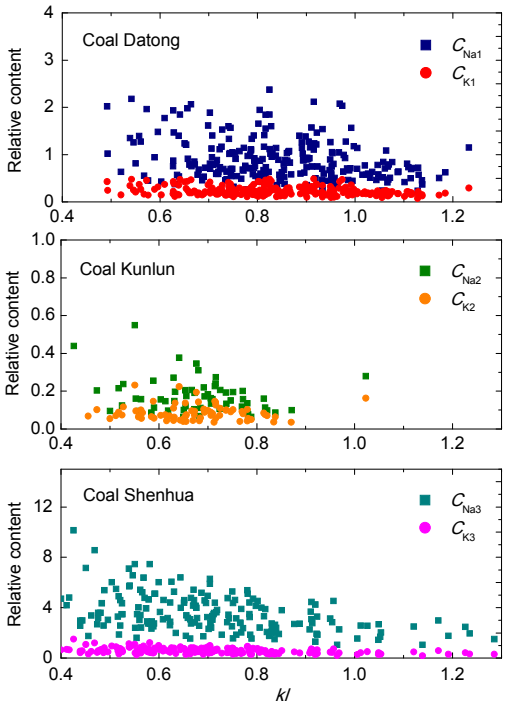

Fig. 7 Relative contents of C_{Na} and C_K versus absorption strength for three coal types

consequently the emitted beam is weakened during its travel from any given point to the edge of the flame (Mavrodineanu and Boiteux, 1965). Therefore, as light travels through the soot particles toward the observer, its intensity decreases exponentially. Empirical absorption compensation factors were found by fitting negative exponential expressions to the experimental data. These were: $B_{Na}=3\exp(-kl/0.75)$, $B_K=3\exp(-kl/0.9)$. The plots of the compensation factors are shown in Figs. 8 and 9.

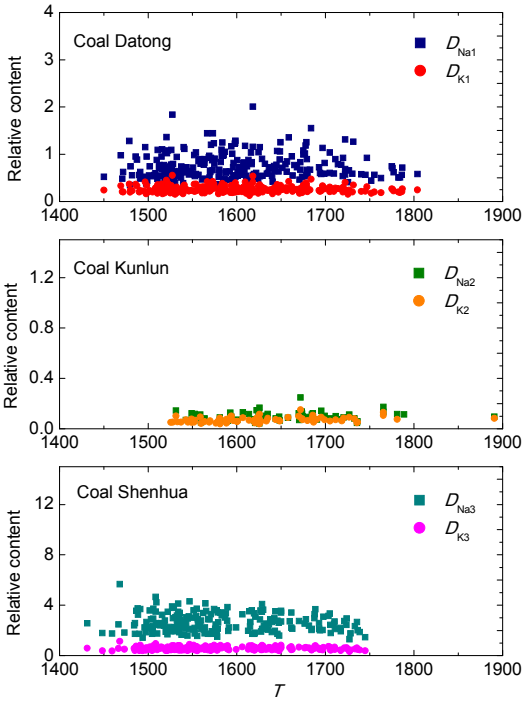

Fig. 8 Compensated relative contents of D_{Na} and D_K versus temperature for three coal types

After compensation, the proportional relationships for the concentrations of Na and K atoms in the flame are $D_{Na}=C_{Na}/(A_{Na}\cdot B_{Na})$ and $D_K=C_K/(A_K\cdot B_K)$. The compensated trends for the three coal types are shown in Figs. 8 and 9. The relationship between Na and K contents is constant at all temperatures and for all soot densities.

Fig. 10 shows the distribution of the D_{Na} and D_K content ratios versus temperature and absorption strength for three coal types. Clearly, the ratio is also a useful indicator of coal type.

The experimental results of three coal types in conditions A and B are shown in Table 4, which are average values of measured results. The results of coal type identification are shown in Fig. 11. The comparison shows that the consistency of the

Table 4 Experimental data of three coal types in conditions A and B

Coal	Condition	T (K)	kl	D_{Na}	D_{Na} scope	D_K	D_K scope	D_{Na}/D_K	(D_{Na}/D_K) scope
Datong	A	1598.6	0.843	0.688	0.425	0.246	0.119	2.781	0.995
	B	1509.6	0.647	0.654	0.387	0.201	0.126	3.263	0.771
Kunlun	A	1536.3	0.545	0.096	0.052	0.072	0.035	1.345	0.403
	B	1589.1	0.657	0.094	0.051	0.051	0.020	1.803	0.433
Shenhua	A	1583.3	0.700	2.535	1.228	0.570	0.247	4.413	0.923
	B	1592.2	0.708	2.031	1.023	0.462	0.190	4.360	0.936

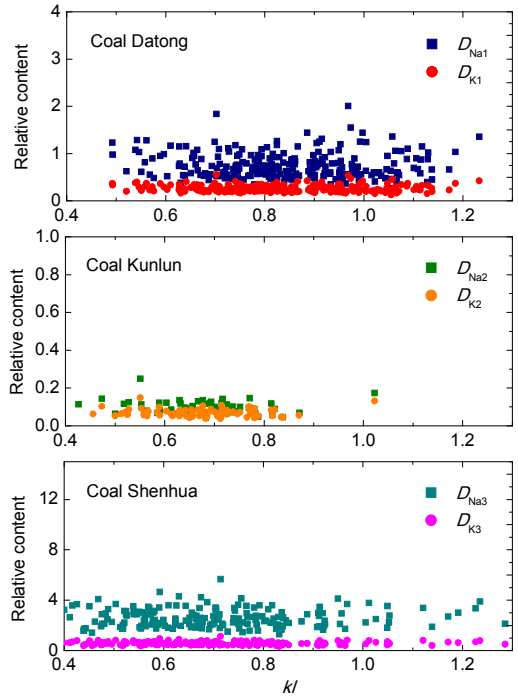

Fig. 9 Compensated relative contents of D_{Na} and D_K versus absorption strength for three coal types

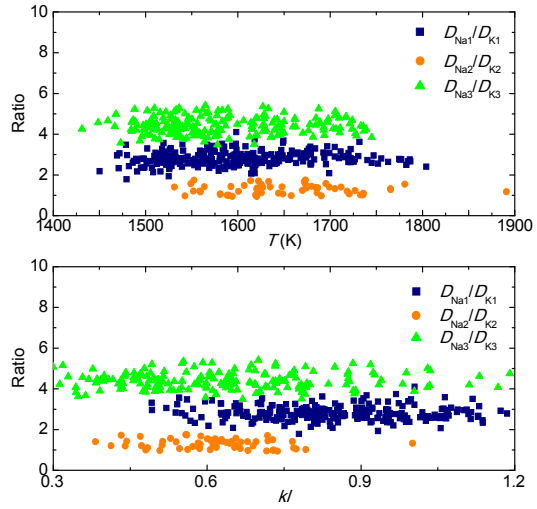

Fig. 10 Content ratios versus temperature and absorption strength for three coal types

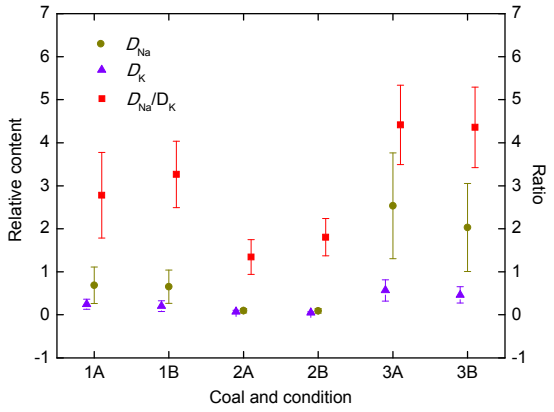

Fig. 11 Coal type identification in different conditions

1A: Coal Datong in condition A; 1B: Coal Datong in condition B; 2A: Coal Kunlun in condition A; 2B: Coal Kunlun in condition B; 3A: Coal Shenhua in condition A; 3B: Coal Shenhua in condition B

characteristic values in different conditions is acceptable. Most core value deviations in two conditions are less than 25%, and the variation ranges of different coals hardly overlap. The characteristic ratios and relative contents of Na and K elements in the flame spectra were stable and identifiable in various conditions. For different coal types, the combination of the ratio and content values were unique across a large range of samples in various conditions. The coal types were identified using automated comparison software.

5 Conclusions

The characteristics of coal flame emission spectra were studied using an experimental apparatus comprising a sedimentation furnace and CCD spectrometer system. The coal flame emission spectra were measured and a novel method was employed to identify coal types in real time, based on calculations

of flame temperature, absorption strength related to soot density, the relative content of vaporized Na and K atoms in the flame, and the ratio between them. Various experimental cases were explored, and a literature survey was carried out. Some concluding remarks can be summarized as follows:

1. The shape of the continuous emission spectrum of the coal flame carries information regarding temperature, emissivity, and soot density. With simplification and using an iterative method, the temperature and absorption strength were calculated correctly and used as the basis for identifying the type of firing coal.

2. The ratio of the intensities of the line spectrum and continuous spectrum at the same wavelength determined from the resonance spectral lines eliminated the influence of flame temperature.

3. Na and K are typical elements vaporized in particles of burning coal, and their presence is clearly seen in the continuous spectrum of a flame. The concentration and proportion of many substances vary with the coal type, including chlorides, sulfates, hydroxides, and Na and K. The Na and K content vaporized in the flame is related to the flame temperature. After temperature compensation, the atomic emission spectra of K and Na are diagnostic properties of the coal type.

4. At a given sampling position, the compensation formula and parameters are the same for all coal types. The temperature compensation formulae are in the form of Arrhenius's equation for reaction rates at different temperatures: A_{Na}=600exp[−83/(RT)], and A_K=300exp[−80/(RT)]. The absorption of light by soot particles is also given by negative exponential compensation equations: B_{Na}=3exp(−kl/0.75), and B_K=3exp(−kl/0.9).

5. After compensation for temperature and the density of soot particles, the relative strength of the Na and K signals and the ratio of one to the other uniquely match the type of coal burnt in various conditions. Further studies are now required to extend the range of the investigation, and to explore the effects of different timing stages of the flames and different fineness as well as humidity of the firing coal.

References

Beatrice, C., Bertoli, C., Cirillo, N.C., *et al.*, 1995. Two-color pyrometry measurements of soot loading in a diesel engine burning model fuels of varying quality. *Combustion Science and Technology*, **110-111**(1):321-339. http://dx.doi.org/10.1080/00102209508951929

Cheng, Z.H., Cai, X.S., Mao, W.P., 2004. Investigate into the characteristic emission line of flame. *Journal of Engineering Thermophysics*, **25**(3):519-522 (in Chinese).

Drake, E., 1996. Atomic, Molecular, and Optical Physics Handbook. AIP Press, Woodbury, USA.

Fu, T.R., Cheng, X.F., Shi, C.L., *et al.*, 2006. The set-up of a vision pyrometer. *Measurement Science and Technology*, **17**(4):659-665. http://dx.doi.org/10.1088/0957-0233/17/4/008

Fu, T.R., Zhao, H., Zeng, J., *et al.*, 2010. Optimization research of three-color pyrometry based on measurement uncertainties. Proceedings of the 9th Asian Thermophysical Properties Conference, No.109276.

Huang, Y., Yan, Y., Riley, G., 2000. Vision-based measurement of temperature distribution in a 500-kW model furnace using the two-colour method. *Measurement*, **28**(3): 175-183. http://dx.doi.org/10.1016/S0263-2241(00)00010-5

Kim, S.S., Kang, Y.S., Lee, H.D., *et al.*, 2012. Release of potassium and sodium species during combustion of various rank coals, biomass, sludge and peats. *Journal of Industrial and Engineering Chemistry*, **18**(6):2199-2203. http://dx.doi.org/10.1016/j.jiec.2012.06.018

Kramida, A., Ralchenko, Y., Reader, J., *et al.*, 2012. NIST Atomic Spectra Database (Version 5.0). National Institute of Standards and Technology, Gaithersburg, USA.

Li, Y., Xiao, J., Zhang, M.Y., 2005. Modeling and prediction of migration mechanism of alkali metals during coal-fired process. *Journal of Fuel Chemistry and Technology*, **33**(5):556-560 (in Chinese).

Lu, S.S., Cheng, X.F., 2003. A fast solution for the primary color measurement method for luminous flames temperature. *Acta Metrologica Sinica*, **24**(4):293-306 (in Chinese).

Mavrodineanu, R., Boiteux, H., 1965. Flame Spectroscopy. Wiley, New York, USA.

Parameswaran, T., Hughes, P.M.J., 2007. Coal flame performance monitoring with flame emission spectroscopy. Third International Conference on Clean Coal Technologies for our Future.

Romero, C., Li, X.C., Keyvan, S., *et al.*, 2005. Spectrometer-based combustion monitoring for flame stoichiometry and temperature control. *Applied Thermal Engineering*, **25**(5-6):659-676. http://dx.doi.org/10.1016/j.applthermaleng.2004.07.020

Schürmann, H., Monkhouse, P.B., 2007. *In situ* parametric study of alkali release in pulverized coal combustion: effects of operating conditions and gas composition. *Proceedings of the Combustion Institute*, **31**(2):1913-1920. http://dx.doi.org/10.1016/j.proci.2006.07.040

Stasio, S., Massoli, P., 1994. Influence of the soot property

uncertainties in temperature and volume-fraction measurements by two-color pyrometry. *Measurement Science and Technology*, **5**(12):1453-1465. http://dx.doi.org/10.1088/0957-0233/5/12/006

Takuwa, T., Naruseb, I., 2007a. Detailed kinetic and control of alkali metal compounds during coal combustion. *Fuel Processing Technology*, **88**(11-12):1029-1034. http://dx.doi.org/10.1016/j.fuproc.2007.06.010

Takuwa, T., Naruseb, I., 2007b. Emission control of sodium compounds and their formation mechanisms during coal combustion. *Proceedings of the Combustion Institute*, **31**(2):2863-2870. http://dx.doi.org/10.1016/j.proci.2006.07.170

Tan, C., Xu, L.J., Cao, Z., 2009. On-line fuel identification using optical sensing and support vector machines technique. Instrumentation and Measurement Technology Conference, p.1144-1147. http://dx.doi.org/10.1109/IMTC.2009.5168450

van Eyk, P.J., Ashman, P.J., Nathan, G.J., 2011. Mechanism and kinetics of sodium release from brown coal char particles during combustion. *Combustion and Flame*, **158**(12):2512-2523. http://dx.doi.org/10.1016/j.combustflame.2011.05.005

Wen, Z.C., Wang, Z.H., Zhou, J.H., *et al.*, 2009. Quantum chemical study on the catalytic mechanism of Na/K on NO-char heterogeneous reactions during the coal reburning process. *Journal of Zhejiang University-SCIENCE A*, **10**(3):423-433. http://dx.doi.org/10.1631/jzus.A0820345

Xu, L.J., Yan, Y., Cornwell, S., *et al.*, 2004. On-line fuel identification using digital signal processing and fuzzy inference techniques. *IEEE Transactions on Instrumentation and Measurement*, **53**(4):1316-1320. http://dx.doi.org/10.1109/TIM.2004.830573

Xu, L.J., Tan, C., Li, X.M., *et al.*, 2012. Fuel-type identification using joint probability density arbiter and soft-computing techniques. *IEEE Transactions on Instrumentation and Measurement*, **61**(2):286-296. http://dx.doi.org/10.1109/TIM.2011.2164836

Zhao, H., Ladommatos, N., 1998. Optical diagnostics for soot and temperature measurement in diesel engines. *Progress in Energy and Combustion Science*, **24**(3):221-255. http://dx.doi.org/10.1016/S0360-1285(97)00033-6

Zhou, H., Li, L.T., Zhang, H.L., *et al*., 2015. Research on the slagging characteristics of blended coals in a pilot-scale furnace. *Journal of Zhejiang University-SCIENCE A (Applied Physics & Engineering)*, **16**(3):204-216. http://dx.doi.org/10.1631/jzus.A1400172

Zizak, G., 2000. Flame Emission Spectroscopy: Fundamentals and Applications. Lecture given at the ICS Training Course on Laser Diagnostics of Combustion Processes, University of Cairo, Egypt.

中文概要

题　目：基于炉膛火焰发射光谱的煤种识别

目　的：为解决煤种频繁变化造成的燃烧闭环优化难题，研究在燃烧器出口实时辨识锅炉入炉燃烧煤种的方法。

创新点：1. 通过火焰发射光谱机理研究获取可排除燃烧工况与测量采样等干扰因素的算法规则；2. 提出基于煤粉火焰光谱中 Na 和 K 元素原子发射光谱相对强度特征的煤种辨识方法。

方　法：1. 通过光纤光谱仪获取锅炉各层燃烧器入口火焰光谱信号；2. 利用同波长下原子光谱与连续辐射光谱的相对关系，消去火焰温度、工况与环境的影响；3. 以补偿后 Na 和 K 元素原子发射光谱强度的特征比值表征不同煤种在火焰中的元素含量特征，实现煤种的在线辨识。

结　论：1. 利用煤粉火焰光谱特征实现入炉煤种的实时辨识具有良好的工况稳定性与可复现性；2. 从算法机理中消除环境影响，降低了测量系统校验的复杂性。

关键词：在线辨识；火焰发射光谱；碱金属；谱线强度